biosensors

MDPI

Article

Biosensor-Monitored Metabolic Effects of Asymmetric Bilateral Hip-Exoskeleton Assistance in Individuals with Transfemoral Amputation

Jiashuo Zhang, Yutong Xi, Yanchen Wu, Hengzhang Wu, Xianyong He and Yixuan Guo *

Department of Mechanical and Energy Engineering, Southern University of Science and Technology, 1088 Xueyuan Blvd, Shenzhen 518055, China
* Correspondence: guoyx@sustech.edu.cn

Abstract

Transfemoral amputation increases the metabolic demands of walking and may impose compensatory loading on the sound side. This study developed an asymmetric bilateral hip-exoskeleton strategy that independently delivered flexion and extension assistance to the prosthetic and sound sides using two-sided Gaussian torque profiles. Three participants walked on a treadmill at self-selected speeds under three conditions: no exoskeleton (No Exo), exoskeleton worn without assistance (Unpowered), and powered assistance (Exo). Wearable biosensors quantified net metabolic power through respiratory gas measurements. In the three analyzed participants, mean net metabolic power during level treadmill walking was 2.06 vs. 2.52 W/kg (Exo versus No Exo). During inclined treadmill walking, the corresponding values were 3.59 vs. 4.38 W/kg. From the supplied participant-level values, mean reductions relative to No Exo were 18.22 ± 0.09% and 18.07 ± 0.49%, respectively. Exo was also lower than Unpowered for every analyzed participant in both tasks. These results indicate that the asymmetric dual-hip assistance monitored by the biosensor is feasible. By reducing walking-related energy expenditure, the proposed exoskeleton may improve walking capacity and thereby enhance quality of life.

Keywords: biosensors; hip exoskeleton; transfemoral amputation

1. Introduction

The effectiveness of walking assistance should be reflected by a reduction in physiological demand when the same motor task is performed. Biosensors and related wearable biosensing technologies can continuously acquire physiological and biochemical information during human movement. They can therefore be used to evaluate the effects of assistive devices on their users [1,2]. In lower-limb amputation research, wearable biosensing and motion-sensing technologies have been combined to characterize locomotion across different tasks. Abarca et al. synchronously collected electromyographic, inertial, and plantar-pressure data from individuals with transtibial amputation and adults without amputation. The dataset covers level walking, ramp ascent and descent, and stair ascent and descent, providing a multimodal resource for gait analysis and locomotion classification [3]. Surface electromyography sensors are commonly used for biosensing. However, amputation results in the loss of residual-limb musculature, which may make electromyographic signals more difficult to acquire and interpret. In individuals with transfemoral amputation, the added mass of the prosthesis and exoskeleton, compensation by the sound side, and the

Check for updates

Received: 24 September 2026
Revised: 16 November 2026
Accepted: 19 November 2026
Published: 24 November 2026

Copyright: © 2026 by the authors. Licensee MDPI, Basel, Switzerland. This article is an open access article distributed under the terms and conditions of the Creative Commons Attribution (CC BY) license.

distribution of bilateral assistance may all alter total energy expenditure. Metabolic measurements reflect the overall energy expenditure of the human body. Cao et al. combined measurements of muscle activity and metabolic cost to evaluate a multi-joint exoskeleton with active–passive assistance. Their study demonstrated how physiological measurements can assess the effects of walking [4]. Therefore, metabolic power was selected as the primary outcome for evaluating the effectiveness of exoskeleton assistance in this study.

As of 2017, more than 57.7 million people worldwide were living with limb amputation [5]. Transfemoral amputation substantially impairs mobility and markedly reduces quality of life [6]. Passive and powered transfemoral prostheses can partially restore knee and ankle function [7,8], but neither fully addresses the demands placed on the hip joints. Passive knee and ankle components cannot generate net positive work; users must therefore advance the prosthesis through residual-limb motion. Compensatory movements of the trunk and intact limb further increase loading on the sound side [9,10]. They may contribute to secondary conditions such as arthritis and back-muscle pain [11,12]. Powered transfemoral prosthetic knees and ankles can generate active power, improve gait symmetry, and reduce the sound-side hip-flexion moment and metabolic cost [13,14]. However, their batteries, actuators, and joint assemblies increase prosthesis mass [15], thereby increasing hip loading on the prosthetic side when advancing the prosthesis. Because distal added mass carries a greater metabolic penalty than mass located near the trunk [16], assistance applied at the hip may provide a valuable complementary approach.

Hip exoskeletons can augment hip-joint function during loaded or unloaded walking [17–22] and have also been investigated for gait rehabilitation in people with walking impairments. Cao et al. developed a hardware circuit system for a soft lower-limb exoskeleton and evaluated its sensor data acquisition, assistance-force tracking, lower-limb muscle activity, and metabolic cost. With powered assistance, net metabolic cost was reduced by 7.8% compared with walking without the exoskeleton [23]. In individuals with chronic post-stroke hemiparesis, bilateral hip assistance has reduced net metabolic cost and positive biological hip work [24]. Rehabilitation training with a hip-exoskeleton system has also improved spatiotemporal gait parameters and between-limb symmetry of muscle activation while reducing net metabolic cost [25]. These findings support the use of hip exoskeletons in populations with asymmetric gait.

Rehabilitation after transfemoral amputation typically includes residual-limb management, preservation of joint range of motion, strengthening, and functional gait training [26]. Loss of distal muscle attachments alters residual-limb morphology and function, and reduced hip-flexion, hip-extension, and hip-abduction moments have been reported on the prosthetic side [27]. Hip-flexion contracture can further complicate prosthetic fitting [28]. These impairments provide a biomechanical rationale for assisting hip flexion and extension during walking.

Powered hip exoskeletons have previously been used for overground gait training in individuals with transfemoral amputation [29–31]. After one month of training with a bilateral active exoskeleton, participants showed improvements in walking distance, walking speed, and cost of transport when subsequently assessed without the device [29,30]. Experiments using the Honda Walking Assist Device likewise showed improvements in self-selected walking speed, stride length, cadence, and hip range of motion [31]. These studies primarily addressed rehabilitation outcomes rather than the immediate metabolic effects of assistance during daily walking.

For immediate walking assistance, Ishmael et al. developed a lightweight unilateral powered hip exoskeleton that synchronized a predefined Gaussian torque profile with gait frequency. In six individuals with above-knee amputation, assistance reduced metabolic cost by 15.6 ± 2.9% [32]. Subsequent biomechanical analysis showed reduced hip effort on

the prosthetic side without substantial changes in gait kinematics or balance, including a 37.5% mean reduction in the prosthetic-side hip-extension moment during early stance [33].

Because individuals with transfemoral amputation may overuse the intact hip to compensate for functional deficits on the prosthetic side [34], bilateral assistance may reduce demands on both limbs. Falls can restrict activity and hinder rehabilitation. Vito et al. used a bilateral hip exoskeleton to counteract balance loss in individuals with transfemoral amputation and reported an effective response in three of five participants [35]. Martini et al. reported metabolic-cost reductions of 5.0% and 3.4% in two participants [36]. Livolsi et al. found that bilateral assistance reduced the physiological cost index relative to transparent mode in four participants, although one participant still had a higher physiological cost index than in the no-exoskeleton condition [37]. These findings indicate that, although an exoskeleton can inject mechanical energy at the hip, the added mass may increase the metabolic cost of walking in some individuals.

Despite this progress, the effects of independently selecting assistance timing and magnitude for the prosthetic and sound sides remain insufficiently characterized. Studies of hip exoskeletons in individuals without amputation have shown that assistance timing, duration, and torque-profile shape influence human–robot energy transfer and metabolic benefit [18,38]. We therefore designed a bilateral hip joint asymmetry assistance strategy for individuals with lower-limb amputation. The assistance timing is when the angular velocity of the thigh swing reaches zero. The assistance curve is an asymmetric two-sided Gaussian assistance profile. Many studies have used symmetrical Gaussian curves as the assistance curve. In this paper, based on the Gaussian curve, considering the human walking cycle, the size of hip joint torque, and the set assistance timing, two different parameter Gaussian curves are used as the assistance curve. The parameter settings of the entire assistance curve are fundamentally different from those in other papers. Oxygen consumption ($\dot{V}O_2$) and carbon dioxide production ($\dot{V}CO_2$) were continuously measured using a portable respiratory-gas-analysis system, and net metabolic power was calculated by indirect calorimetry [39]. These biosensor-based measurements were used to quantify the metabolic effects of the proposed assistance method during level-ground and ramp-ascent walking. This study aimed to evaluate the effects of the proposed method on the metabolic cost of walking at self-selected speeds and self-selected slope gradients. The aim was to provide experimental evidence for investigating the biomechanical mechanisms of bilateral hip-exoskeleton assistance during daily walking in individuals with transfemoral amputation.

2. Materials and Methods

2.1. Hardware Setup

The bilateral hip-exoskeleton prototype had a total mass of 3.7 kg (Figure 1). Its nylon structure extended from the posterior trunk to both thighs through curved members. The system comprised a main controller, a battery, bilateral hip actuators, waist and thigh attachments, and bilateral IMUs. An STM32F427IIH6 development board mounted on the back served as the main controller. Each hip actuator used a GO-M8010-6 brushless motor with a maximum output torque of 23.7 Nm and a torque-control accuracy of approximately 0.03 Nm. The actuators communicated with the controller through RS485. JY901B IMUs sampled thigh-motion signals at 200 Hz and communicated through UART. A host–computer interface connected through UART or Bluetooth and displayed sensor signals, assistance-trigger events, and torque commands in real time.

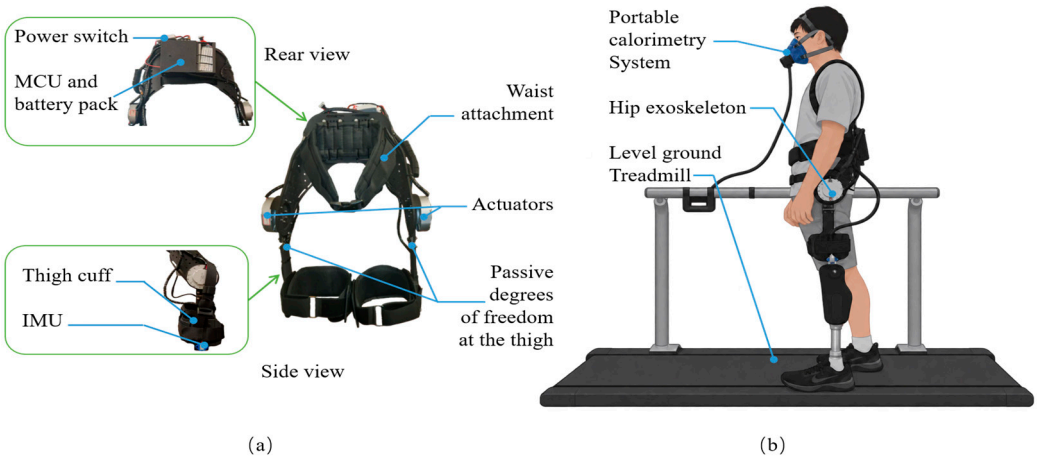


Figure 1. (**a**) Exoskeleton and its hardware system; (**b**) biosensing evaluation system based on metabolism.

Figure 2 summarizes the assistance-control framework. IMUs mounted on both thighs measured sagittal-plane thigh angular velocity, and the signals were low-pass-filtered before gait-event detection. Angular-velocity zero-crossings were used to identify transitions between forward and backward thigh motion. The controller then generated the desired hip torque from the predefined assistance profile, and the bilateral actuators applied the corresponding commands. Assistance timing and torque-profile parameters were independently adjustable for the prosthetic and sound sides. Initial parameters were obtained from a backpropagation neural network model and subsequently fine-tuned during participant familiarization.

2.2. Assistance Control Strategy

The control strategy comprised two components: event-based assistance timing and generation of the desired torque profile. Transitions between hip-flexion and hip-extension assistance were identified from sign changes in filtered sagittal-plane thigh angular velocity. For each limb, the detected event initiated a predefined asymmetric torque profile whose amplitude, peak phase, and rising and falling widths could be adjusted independently, thereby enabling asymmetric bilateral assistance. In this study, negative exoskeleton torque denotes hip-flexion assistance, whereas positive exoskeleton torque denotes hip-extension assistance. The Gaussian model predicts the nonnegative torque magnitude, and the torque direction is assigned separately according to the active assistance state.

2.2.1. Assistance Timing

During steady-state walking, lower-limb motion is approximately periodic [40]. Controllers based on predefined assistive torques commonly use a recurring gait event, such as heel strike, to reset the assistance cycle. Because transfemoral amputation removes part of the thigh musculature, the residual limb is weakened. Whether a passive or powered prosthesis is used, the prosthetic side must move the residual limb and transfemoral prosthesis toward their maximum forward angle after the stance phase begins. This action requires sufficient hip torque to bring the residual limb and prosthesis toward the pre-amputation thigh angle. Some individuals therefore generate compensatory effort at the intact hip to increase the swing angle of the prosthetic side. From the maximum forward-swing angle until prosthetic heel contact, gravity can assist the downward motion of the prosthetic side. Accordingly, the first hip-exoskeleton assistance phase corresponded to forward swing of the prosthetic side, encompassing early and mid-swing, whereas the second phase corresponded to limb descent and support, encompassing late swing and stance. Figure 3 shows

the ideal correspondence between these two assistance phases and hip-torque demand. Because gait patterns and walking habits vary among individuals, the exoskeleton assistance peak cannot be precisely aligned with every user's biological torque peak. The asymmetric Gaussian assistance profile was therefore designed to rise rapidly after triggering so that the assistance peak would occur close to the peak of the user's biological effort.

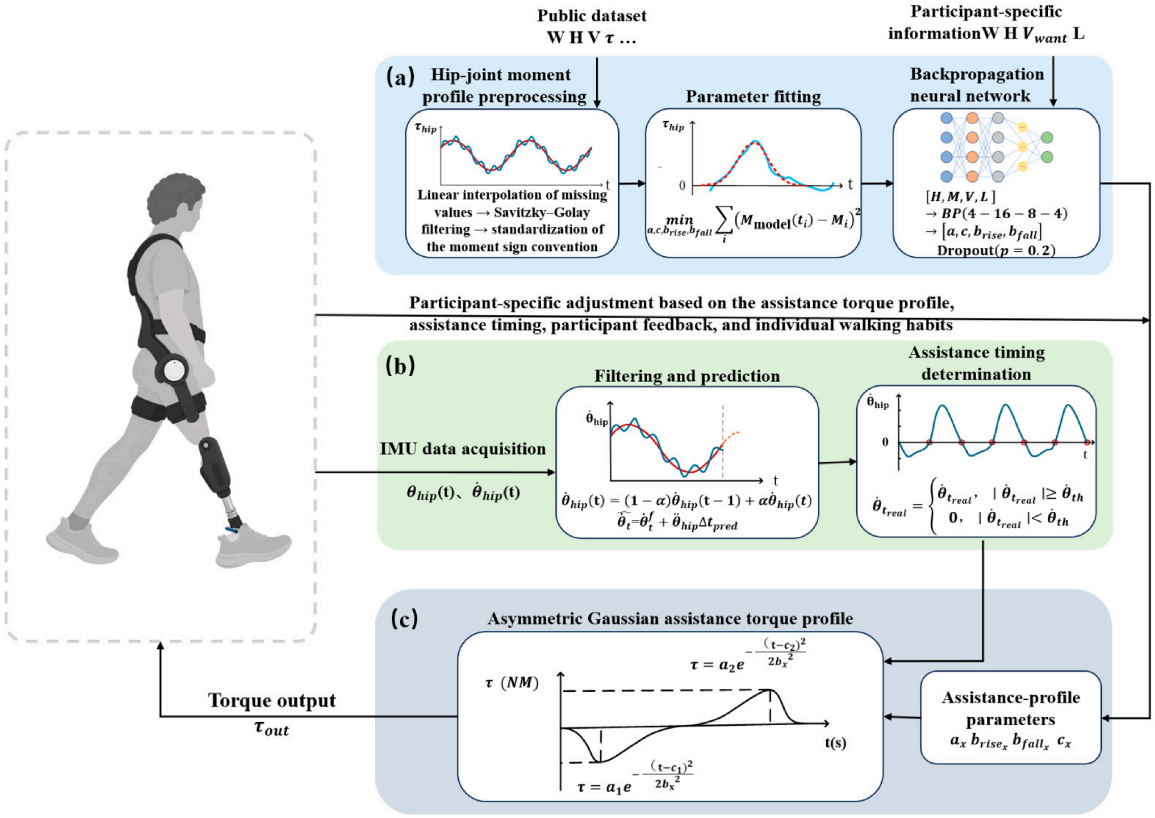


Figure 2. Logic diagram of bilateral hip-exoskeleton assistance for participant with transfemoral amputation. (**a**) Construction of the participant-specific hip-joint moment profile; the blue curve represents the raw data and the orange curve the processed data. (**b**) IMU-based estimation of gait phase and assistance timing; the blue curve represents the raw data, the solid orange curve the processed data, and the dashed orange curve the predicted data. (**c**) Generation of the asymmetric Gaussian assistance torque profile; the curve represents the output torque.

Specifically, a zero-crossing of hip angular velocity was used as the gait event marking the start and end of an assistance phase. Figure 4 presents the hip-flexion assistance logic. Forward thigh motion was defined as positive and backward motion as negative. A negative-to-positive crossing triggered hip-flexion assistance, whereas a positive-to-negative crossing terminated flexion assistance and initiated the hip-extension assistance state. Because the prosthetic and sound sides used the same trigger logic and differed only in selected parameters, only the hip-flexion trigger is described in detail. The hip-flexion assistance logic was as follows:

$$T_q = \begin{cases} M_q(t),\ q_f = 1 \\ 0,\ q_f = 0 \vee t_{real} - t_{startq} > T_{max} \end{cases} \quad (1)$$

$$q_f = \begin{cases} 1,\ \text{if } \dot{\theta}_{t_{real}} \geq 0,\ \dot{\theta}_{t_{real-1}} < 0 \text{ and } T_{max} > t_{real} - t_{startq} > T_{min} \\ 0,\ \text{if } \dot{\theta}_{t_{real}} \leq 0 \text{ and } \dot{\theta}_{t_{real-1}} > 0 \end{cases} \quad (2)$$

$$\dot{\theta}_{t_{real}} = \begin{cases} \dot{\theta}_{t_{real}},\ |\dot{\theta}_{t_{real}}| \geq \dot{\theta}_{th} \\ 0,\ |\dot{\theta}_{t_{real}}| < \dot{\theta}_{th} \end{cases} \quad (3)$$

where $M_q(t)$ is the desired hip-flexion torque; q_f is the hip-flexion state parameter; t_{real} is the program running time; t_{startq} is the start time of hip-flexion assistance, namely the time when q_f changes from 0 to 1; t_{endq} is the end time of hip-flexion assistance, namely the time when q_f changes from 1 to 0; T_{max} is the maximum assistance duration; T_{min} is the minimum window period; $\dot{\theta}_{t_{real}}$ is the angular velocity at the current time; and $\dot{\theta}_{th}$ is the angular-velocity zero threshold.

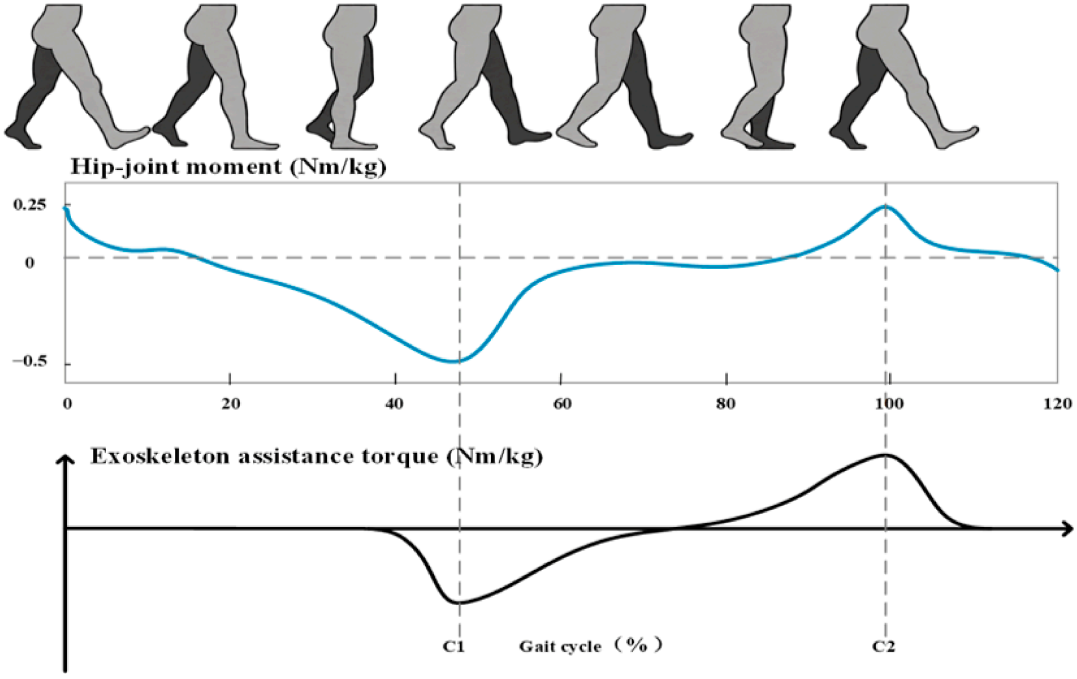


Figure 3. Ideal correspondence between prosthetic-side hip-joint torque and assistance timing.

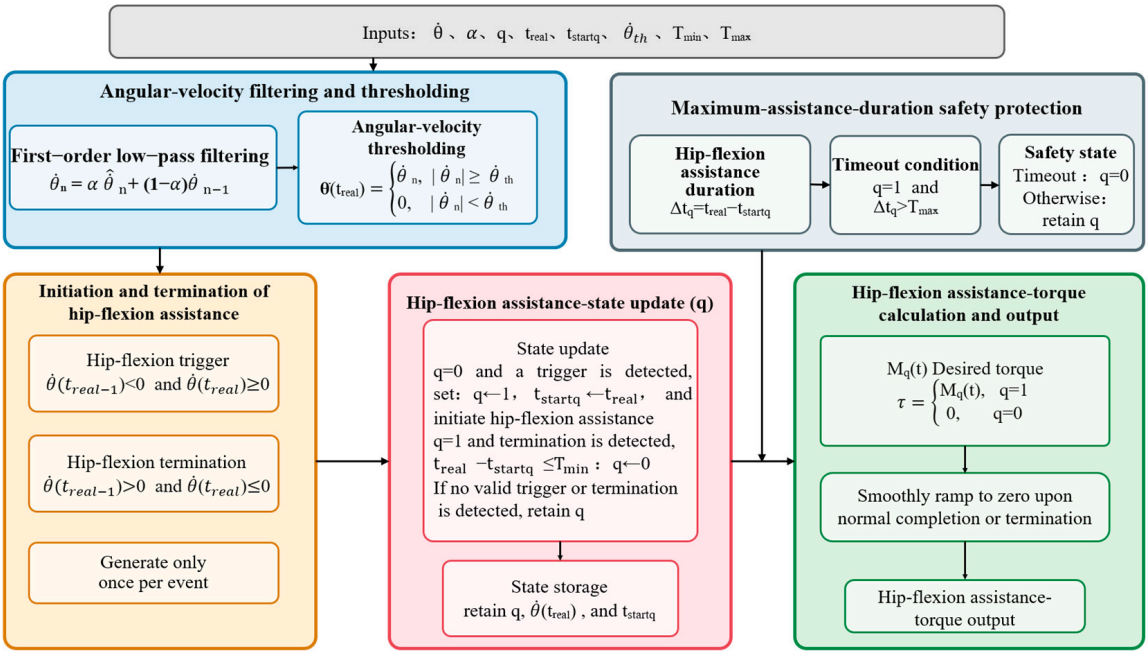


Figure 4. Logic diagram of assistance-timing determination.

The hip-flexion state was updated according to the following rules: samples satisfying $|\dot{\theta}_{t_{real}}| < \dot{\theta}_{th}$ were treated as belonging to a zero-velocity region and were not used alone to switch states; for the flexion trigger, when $q_f = 0$ and the filtered thigh angular velocity

crossed from negative to positive, recorded as $t_{startq} = t_{real}$, then $q_f = 1$ was set, and flexion assistance was initiated on that side; for flexion termination, when $q_f = 1$ and angular velocity crossed the zero region from positive to negative, recorded as $t_{endq} = t_{real}$, then $q_f = 0$ was set, and a smoothing segment was applied before terminating the flexion assistance; to reduce false triggers caused by impact, vibration, or sensor noise, new zero-crossing events were ignored during a minimum refractory window; if an assistance state exceeded the maximum allowed duration, then the controller reset the state and terminated assistance through the same smoothing procedure.

In addition, because angular velocity fluctuates around zero during standing and slow walking, direct zero-crossing detection can cause false triggers. To balance stability and real-time responsiveness, a first-order low-pass filter was applied to the angular-velocity signal.

$$\dot{\theta}_n = \alpha\tilde{\dot{\theta}}_n + (1 - \alpha)\dot{\theta}_{n-1} \quad (4)$$

where n denotes the discrete-time index, $\tilde{\dot{\theta}}_n$ is the current sampled angular velocity, $\dot{\theta}_n$ is the filtered angular velocity, and α is the filtering weight.

2.2.2. Assistance Torque Curve Based on an Asymmetric Gaussian Model

Predefined hip-exoskeleton torque profiles are commonly represented by symmetric functions, including Gaussian curves [12]. In the present controller, however, assistance was triggered by reversals in thigh motion, at which point the biological hip moment was nonzero [41]. We therefore used an asymmetric two-sided Gaussian function as the predefined assistance torque profile. This torque is a piecewise function of time t and allows the assistance torque to rise rapidly after triggering, better matching biological effort. The same asymmetric two-sided Gaussian form was used for the swing and stance phases, with different parameter values. Figure 5 illustrates the exoskeleton torque profile formed by connecting hip-flexion and hip-extension assistance. With the peak phase as the boundary, each assistance profile consists of two independently defined Gaussian segments. The function for one assistance phase is:

$$M(t_n) = \begin{cases} ae^{-\frac{(t_n - c)^2}{2b_{rise}^2}}, & \text{if } 0 \le t_n \le c \\ ae^{-\frac{(t_n - c)^2}{2b_{fall}^2}}, & \text{if } c < t_n \end{cases} \quad (5)$$

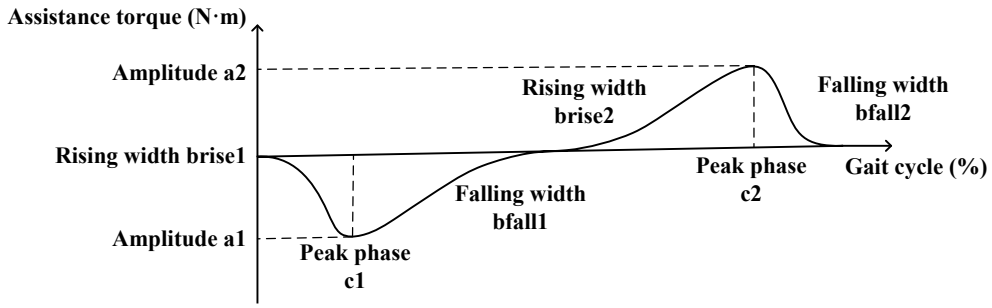


Figure 5. Schematic diagram of the asymmetric two-sided Gaussian assistance torque curve and parameter definitions.

Parameter a defines the peak torque amplitude; c defines the phase of peak assistance; b_{rise} controls the width of the rising portion; and b_{fall} controls the width of the falling portion. Here, t_n denotes time normalized to the gait-cycle phase, with values ranging from 0 to 1. The unit of parameter a is Nm/kg, while the units of parameters c, b_{rise}, and b_{fall} are normalized to the range of 0–1 and are dimensionless. Multiply the normalized biological moments by the mass of each subject to obtain the assistance torque. The filter is a low-pass

filter with a filter weight of 0.015, a detection threshold of 3°/s, a refractory window of 350 ms, and the termination smoothing time of 50 ms. The maximum assistance duration is 500 ms.

2.3. Initialization Fitting of Assistance-Curve Parameters Based on a Backpropagation Neural Network

Predefined torque-profile parameters can be adjusted empirically [32], but this approach depends strongly on researcher experience, requires substantial tuning time, and has limited adaptability across participants. We therefore used an intelligent parameter-prediction scheme based on a backpropagation (BP) neural network to assist parameter selection. As shown in Figure 6, the network was trained using the public gait dataset reported by Hussain and Marmar [41]. Inputs included height (H), body mass (W), walking speed (V), and limb category (L). Sagittal-plane hip-moment trajectories were preprocessed to address missing values, smooth the signals, and standardize the sign convention. Selected trajectory intervals were then fitted to the asymmetric two-sided Gaussian model by least squares, yielding a, c, b_{rise}, and b_{fall} as prediction targets. Standardized inputs were passed through two fully connected hidden layers with dropout, and the output layer constrained predicted parameters to nonnegative values. The BP neural network used a 4–16–8–4 network. Height, body mass, and walking speed were standardized. The four fitted profile targets were scaled to 0.1–1.0 before training. ReLU was used in both hidden layers, dropout of 0.2 followed the first layer, and Softplus constrained the four outputs to positive values. The archived script used mean-squared-error loss with Adam (learning rate 0.001, weight decay 10^{-4}) for 1500 full-batch epochs. The model outputs were used only as initial estimates. An experimenter subsequently fine-tuned the assistance parameters while reviewing IMU signals, trigger timing, commanded torque, and participant feedback. Figure 7 shows representative fits for the prosthetic and sound sides of two participants in the dataset. AMPF2 and AMPM3 are the original participant identifiers used in the source dataset, denoting a female and a male participant with transfemoral amputation, respectively.

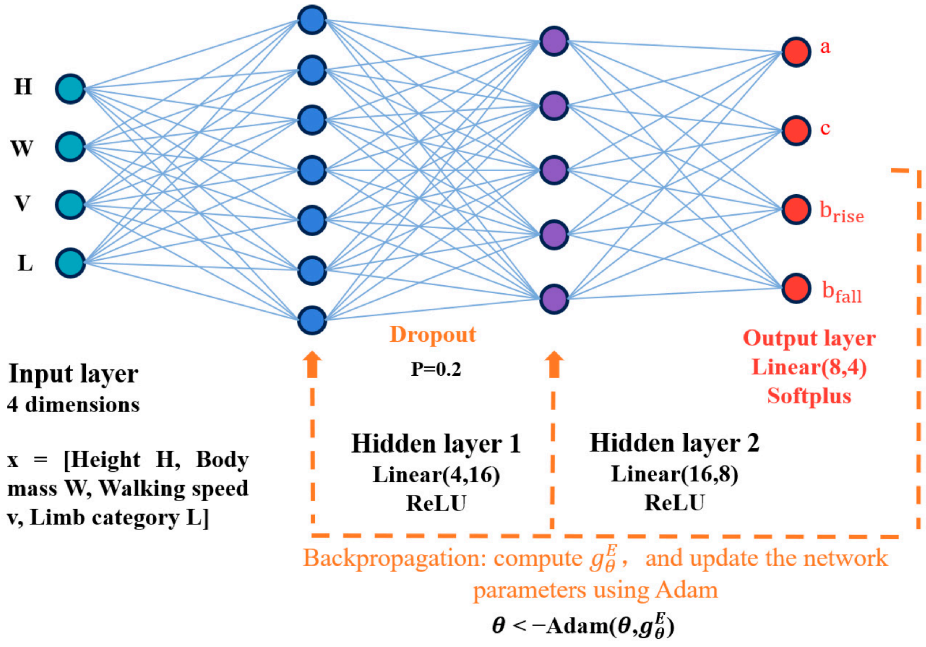


Figure 6. Parameter-initialization process of the BP neural network.

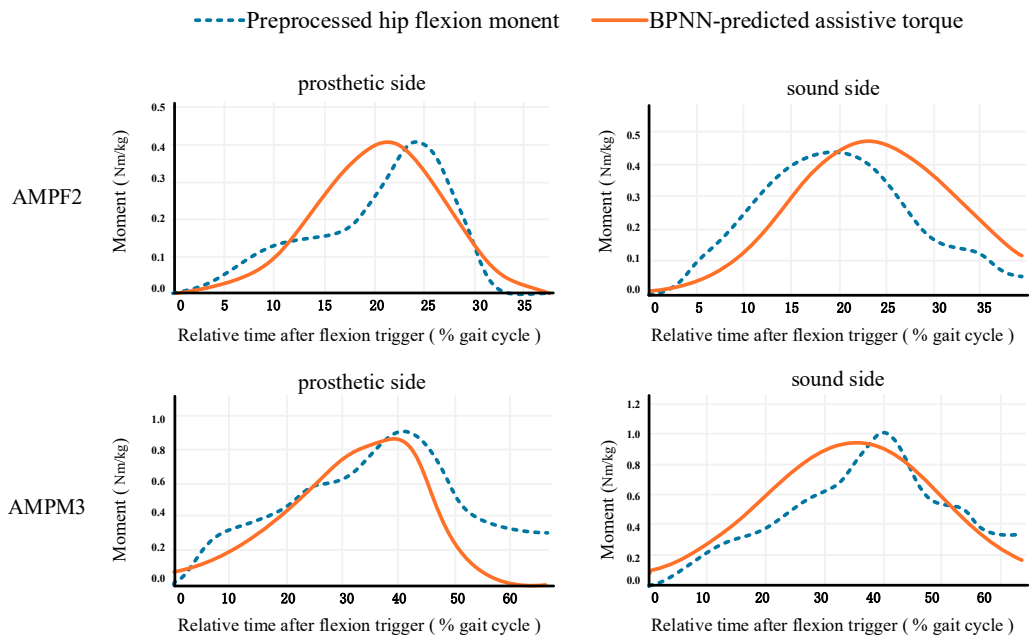


Figure 7. Examples of partial fitting results.

The two limbs used the same event-detection and torque-generation framework, but their IMU signals, state variables, and assistance parameters were updated independently. This architecture allowed limb-specific tuning while retaining a common monitoring interface.

2.4. Experimental Protocol

2.4.1. Participant Recruitment and Ethics

Adults who routinely used a unilateral transfemoral prosthesis were recruited. Inclusion criteria were as follows: age, 18–50 years; unilateral transfemoral amputation for at least 6 months; daily use of usual passive prosthesis; the ability to walk continuously for 6 min on a treadmill or level surface. Exclusion criteria included severe cardiopulmonary or neuromuscular disease, severe skin or vascular disorders, residual-limb pain, poor socket fit, elevated recent fall risk, inability to communicate with the research team, or another condition judged by a physician or the study lead to preclude safe participation.

The participants' details are listed in Table 1. Subject 1, Subject 2, Subject 3, and Subject 4 denote participant identifiers, and the asterisk indicates that a participant's data were abnormal and excluded from analysis. The K-level denotes Medicare Functional Classification Level; MPK denotes a microprocessor-controlled prosthetic knee; Mech denotes a mechanical prosthetic knee; ESAR denotes an energy-storing-and-return prosthetic foot; and Rigid denotes a rigid prosthetic foot. Time since amputation and duration of prosthesis use are also reported. None of the participants had previous experience with a powered exoskeleton.

2.4.2. Level Ground Metabolic Experiment

Oxygen consumption ($\dot{V}O2$) and carbon dioxide production ($\dot{V}CO2$) were measured using a portable metabolic system (K5, COSMED), and the breath-by-breath (B × B) mode was used. The system was calibrated one day before each experiment. Participants fasted for at least 2 h before testing to minimize shifts in metabolic expenditure caused by food intake. Height, body mass, age, amputation side, time since amputation, prosthesis type, K-level, and self-selected walking speed were recorded. Among these variables, height, body mass, walking speed, and limb category were used as inputs to the neural network

model to obtain initial estimates of a, c, b_{rise}, and b_{fall}. The exoskeleton was then fitted, and the waist, shoulder, and thigh attachments were adjusted to minimize discomfort and the relative motion between the exoskeleton and the prosthetic socket.

Table 1. Participant information.

	Subject 1	Subject 2	Subject 3	Subject 4 *
Age [year]	40	46	27	35
Sex	female	male	male	male
Height [m]	1.6	1.69	1.78	1.72
Body mass [kg]	56.5	62	65	85
K-Level	K2	K3	K3	K3
Prosthetic knee	MPK	Mech	MPK	MPK
Prosthetic foot	Rigid	ESAR	Rigid	ESAR
Amputation [year]	9	26	13	28
Prosthesis [year]	4	26	13	18

The asterisk indicates that a participant's data were abnormal and excluded from analysis.

After the exoskeleton was fitted, the experimenter fine-tuned the assistance parameters while monitoring thigh angular velocity, trigger timing, commanded torque, and participant feedback. The final parameter set for each participant was held constant throughout the experiment. Before formal testing, participants completed approximately 30 min of familiarization walking.

After parameter tuning and familiarization walking, participants rested for 20 min. At the beginning of testing, each participant stood quietly for 6 min while resting metabolic power was measured using the wearable biosensing system. Participants then completed 6 min treadmill trials at a fixed self-selected speed under three conditions: No Exo, Unpowered, and Exo. Condition order was randomized, and consecutive trials were separated by at least 10 min of rest. Mean $\dot{V}O_2$ and $\dot{V}CO_2$ over the final 4 min of each trial were used to calculate body-mass-normalized net metabolic power. We selected the final four minutes as the averaging window because metabolic measurements may not have reached a steady state during the first two minutes of walking [42].

$$\text{Metabolic Power} = \frac{16.58\dot{V}O_2 + 4.51\dot{V}CO_2}{m} \quad (6)$$

where $\dot{V}O_2$ and $\dot{V}CO_2$ are expressed in mL/s, and m denotes body mass in kilograms. Gross metabolic power was estimated from the respiratory-gas data measured by the biosensing system using the indirect-calorimetry equation above. Net metabolic power was calculated by subtracting quiet-standing metabolic power from the gross metabolic power measured during walking. After testing, participants provided qualitative feedback regarding comfort and perceived effects on gait and walking effort.

2.4.3. Ramp Ascent Metabolic Experiment

To explore performance beyond level-ground walking, participants repeated the metabolic protocol during treadmill ramp-ascent walking. The biosensing system and walking speed were kept the same as in the level-ground condition. The slope gradient of the treadmill was set by each participant themselves in a comfortable walking state and remained constant throughout the experiment. Participant-specific speeds and slope gradient are listed in Table 2.

Table 2. Experimental data.

Walking Information	Subject 1	Subject 2	Subject 3
Velocity [m/s]	0.4	0.7	0.6
Angle [°]	3	5	4

The ramp ascent protocol (Figure 8) used the same three conditions, randomized condition order, 6 min trial duration, minimum 10 min rest interval, and metabolic-data processing procedure as the level ground protocol. Assistance timing and profile-shape parameters were unchanged from level-ground walking; only torque amplitude was adjusted for ramp-ascent walking.

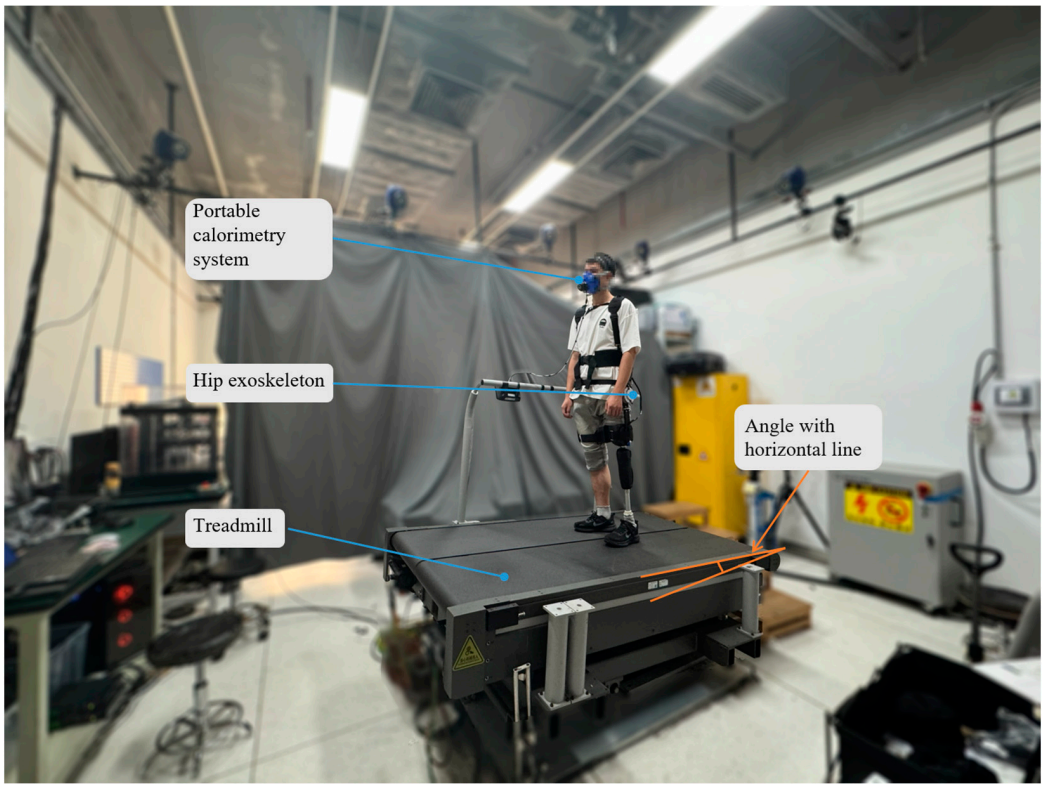


Figure 8. Ramp ascent experimental platform.

3. Results

Three of the four recruited participants completed the protocol and contributed metabolic results. Subject 4 had a short residual limb and a high amputation level. During the experiment, it was observed that there was a significant gap between the binding and the receiving cavity, preventing the effective transmission of torque. Even after adjustments, there was still no significant improvement, so the experiment was terminated. This was a hardware-fit failure, rather than exclusion of an unfavorable metabolic response. No comparable attachment failure occurred for the other three participants.

During level-ground treadmill walking, net metabolic power in the three analyzed participants was 2.52 ± 0.59 W/kg in No Exo, 2.83 ± 0.68 W/kg in Unpowered, and 2.06 ± 0.48 W/kg in Exo (mean ± SD; corresponding SEMs: 0.34, 0.39, and 0.27 W/kg, respectively; Figure 9a). Relative to No Exo, the participant-level reductions with Exo were 18.21%, 18.37%, and 18.06% for Subjects 1–3, respectively, with a mean reduction of 18.22% (SD: 0.16%; SEM: 0.09%). All three participants showed a reduction in net metabolic power with powered assistance. These results indicate that active assistance compensated for part

of the metabolic burden associated with the added mass of the exoskeleton. They also indicate a further reduction in net metabolic power during level-ground walking.

During ramp-ascent treadmill walking at each participant's selected inclination, net metabolic power was 4.38 ± 1.36 W/kg in No Exo, 4.94 ± 1.29 W/kg in Unpowered, and 3.59 ± 1.12 W/kg in Exo (mean ± SD; corresponding SEMs: 0.79, 0.75, and 0.65 W/kg, respectively; Figure 9b). Relative to No Exo, the participant-level reductions with Exo were 17.19%, 18.10%, and 18.90% for Subjects 1–3, respectively, with a mean reduction of 18.07% (SD: 0.85%; SEM: 0.49%). The direction of change was consistent across all three participants. These results indicate that the proposed bilateral hip-exoskeleton assistance method also reduces in net metabolic power during ramp-ascent walking.

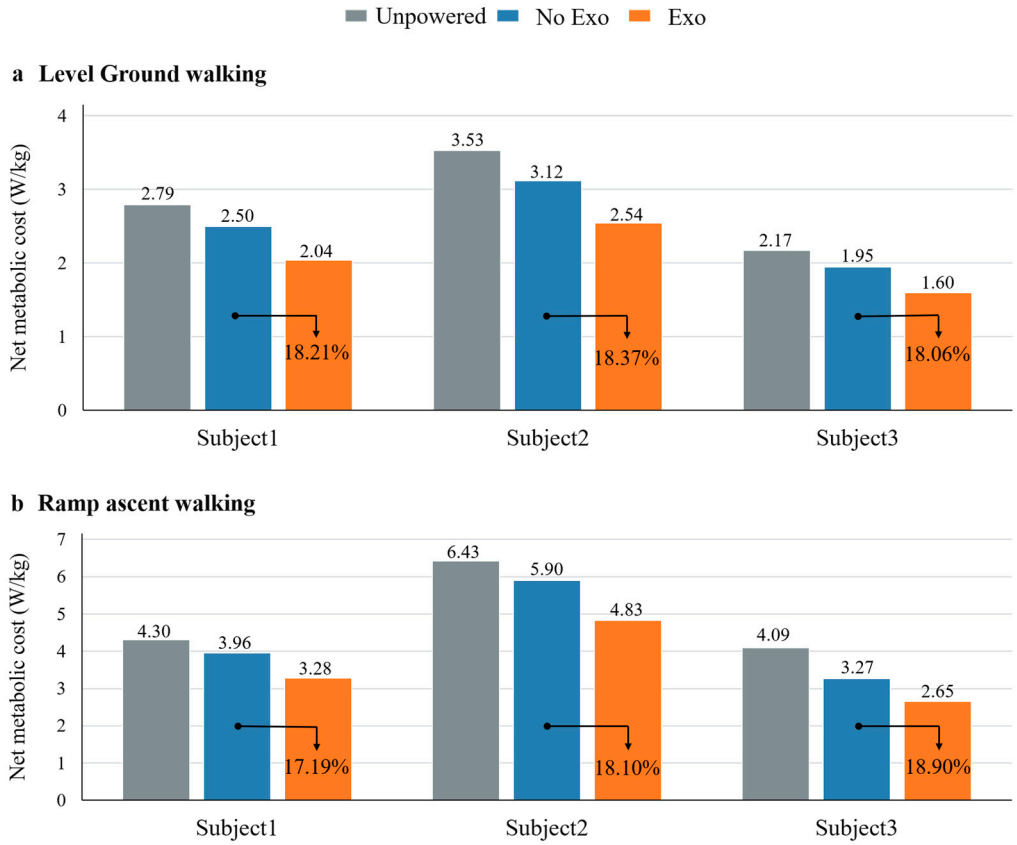


Figure 9. Net metabolic power under different exoskeleton conditions. (**a**) Level-ground walking; (**b**) Ramp-ascent walking. (To facilitate the presentation of some data, only two decimal places are retained. The reduction amount was calculated based on the original data.)

All percentage reductions and summary statistics for both walking tasks were calculated from the participant-level W/kg values before rounding; therefore, recalculation from values displayed to two decimal places may produce small differences.

4. Discussion

Across both walking protocols, wearing the unpowered exoskeleton increased net metabolic power relative to No Exo, whereas powered assistance reduced net metabolic power relative to both No Exo and Unpowered. This pattern indicates that active hip assistance offset the metabolic cost of carrying the exoskeleton in the three participants who completed the protocol. The assistance torques used in testing were below 12 Nm, lower than the actuator's maximum output torque of 23.7 Nm. Reducing the required maximum torque would allow the use of a lighter motor, helping to decrease exoskeleton mass and the associated metabolic cost and potentially producing a greater assistance benefit.

Four participants were initially recruited, but abnormal data were obtained from participant Subject 4. This participant had a high amputation level and a short residual limb. When the bilateral hip exoskeleton was worn, the thigh attachment tended to detach, and the exoskeleton body slipped relative to the prosthetic socket, reducing effective transmission of the assistance torque. During the 6 min self-selected-speed walking trial, the prosthetic-side thigh attachment detached after approximately 2 min. Effective assistance could no longer be provided; instead, the device interfered to some extent with the participant's natural gait, and an adequate duration of valid assisted data could not be obtained. The participant was therefore excluded according to the exclusion criteria. No such problem occurred in the other participants. The current hip-exoskeleton prototype requires improvement in its adaptability to different residual-limb lengths and prosthetic-socket shapes. Insufficient compatibility between the thigh attachment and the user can reduce the transmission efficiency of the exoskeleton output torque. Whether assistance effectiveness differs among individuals with different residual-limb lengths is one direction for future research.

All participants reported that walking felt easier with powered assistance and perceived that they could walk faster and for longer periods. Although these reports were encouraging, walking speed and endurance were not objectively evaluated in the present study, and further quantitative assessment is needed.

Comparison with prior work: Ishmael et al. reported a 15.6 ± 2.9% (mean ± SEM) metabolic reduction with unilateral residual-hip assistance during treadmill walking [32]. Martini et al. reported 5.0% and 3.4% reductions in two participants with an active pelvis orthosis in a treadmill metabolic protocol [36]. Livolsi et al. studied bilateral assistance using the physiological cost index and overground walking [37]; these PCI values are not directly interchangeable with our respiratory-gas-derived W/kg values. The new knowledge contributed by our research lies in proposing a new bilateral hip joint assistance strategy for unilateral transfemoral amputees who wear prosthetic limbs. The limitation is that only three subjects completed the test and biomechanical information such as hip joint torque was not collected.

Future work should examine participants with a wider range of characteristics, including different K-levels and residual-limb lengths, and should incorporate biomechanical measures such as hip-joint moment and joint range of motion. Future studies should also combine respiratory-gas biosensing with other wearable biosensing modalities, such as surface electromyography, plantar-pressure sensing, and cardiovascular monitoring. Multimodal measurements could help distinguish whole-body metabolic benefits from limb-specific compensation and clarify how assistance timing and amplitude affect physiological responses. Future work should investigate whether biosensor-informed parameter optimization can improve individualized assistance outcomes. It should also explore the combined use of a hip exoskeleton and a powered knee–ankle prosthesis.

5. Conclusions

This study implemented asymmetric bilateral hip assistance using limb-specific motion-reversal triggering and two-sided Gaussian torque profiles. Wearable respiratory biosensors quantified metabolic outcomes, while a BP neural network supplied initial parameters before manual tuning. During level-ground walking, the three analyzed participants' net metabolic power was 2.52 ± 0.34, 2.83 ± 0.39, and 2.06 ± 0.27 W/kg in the No Exo, Unpowered, and Exo conditions, respectively. Exo reduced net metabolic power by 18.22 ± 0.09% relative to No Exo. During ramp ascent, the corresponding values were 4.38 ± 0.79, 4.94 ± 0.75, and 3.59 ± 0.65 W/kg, with an 18.07 ± 0.49% reduction for Exo relative to No Exo. These findings support the feasibility of the proposed assistance strategy and suggest its potential to make walking less physiologically demanding, which may in turn support walking endurance. A

participant with a short residual limb experienced attachment-fit difficulties. Future work should improve attachment compatibility and incorporate biomechanical measurements to investigate the mechanisms underlying the observed reductions in metabolic cost.

Author Contributions: Conceptualization, Y.G.; methodology, J.Z. and Y.G.; validation, H.W. and X.H.; formal analysis, J.Z. and Y.W.; investigation, Y.X.; writing—original draft preparation, J.Z.; writing—review and editing, J.Z., Y.X., Y.W., H.W., X.H. and Y.G.; project administration, Y.G.; funding acquisition, Y.G. All authors have read and agreed to the published version of the manuscript. All authors have read and agreed to the published version of themanuscript.

Funding: This research was funded by Shenzhen Science and Technology Program under Grant JCYJ20230807093407016, Guangdong Basic and Applied Basic Research Foundation under Grant 2023A1515110779, National Natural Science Foundation of China under Grant 62403230 and SUSTech Undergraduate Innovation and Entrepreneurship Training Program, grant number S202614325031.

Institutional Review Board Statement: The study was conducted in accordance with the Declaration of Helsinki, and approved by the Institutional Review Board at Southern University of Science and Technology (protocol code 20230111).

Informed Consent Statement: Informed consent was obtained from all subjects involved in the study. Written informed consent has been obtained from the patient(s) to publish this paper.

Data Availability Statement: Data available upon request.

Acknowledgments: During the preparation of this manuscript, the authors used ChatGPT (OpenAI; GPT-6) for the purposes of check grammar, spelling, and punctuation. The authors have reviewed and edited the output and take full responsibility for the content of this publication.

Conflicts of Interest: The authors declare no conflicts of interest.

References

1. Kim, J.; Campbell, A.S.; Esteban-Fernández de Ávila, B.; Wang, J. Wearable biosensors for healthcare monitoring. *Nat. Biotechnol.* **2019**, *37*, 389–406. [CrossRef] [PubMed]
2. Ye, S.; Feng, S.; Huang, L.; Bian, S. Recent progress in wearable biosensors: From healthcare monitoring to sports analytics. *Biosensors* **2020**, *10*, 205. [CrossRef] [PubMed]
3. Abarca, V.E.; Chavez, J.; Eulogio, L.; Viviano, C.; Elias, D.A. Multimodal biomechanical dataset from transtibial amputees and able-bodied adults across five locomotion tasks. *Sci. Data* **2026**, *13*, 155. [CrossRef] [PubMed]
4. Cao, W.; Zhang, Z.; Chen, C.; He, Y.; Wang, D.; Wu, X. Biomechanical and Physiological Evaluation of a Multi-Joint Exoskeleton with Active-Passive Assistance for Walking. *Biosensors* **2021**, *11*, 393. [CrossRef] [PubMed]
5. McDonald, C.L.; Westcott-McCoy, S.; Weaver, M.R.; Haagsma, J.; Kartin, D. Global prevalence of traumatic non-fatal limb amputation. *Prosthet. Orthot. Int.* **2021**, *45*, 105–114. [CrossRef] [PubMed]
6. Wurdeman, S.R.; Stevens, P.M.; Campbell, J.H. Mobility Analysis of AmpuTees (MAAT I): Quality of life and satisfaction are strongly related to mobility for patients with a lower limb prosthesis. *Prosthet. Orthot. Int.* **2018**, *42*, 498–503. [CrossRef] [PubMed]
7. Versluys, R.; Beyl, P.; Van Damme, M.; Desomer, A.; Van Ham, R.; Lefeber, D. Prosthetic feet: State-of-the-art review and the importance of mimicking human ankle-foot biomechanics. *Disabil. Rehabil. Assist. Technol.* **2009**, *4*, 65–75. [CrossRef] [PubMed]
8. Gehlhar, R.; Tucker, M.; Young, A.J.; Ames, A.D. A review of current state-of-the-art control methods for lower-limb powered prostheses. *Annu. Rev. Control* **2023**, *55*, 142–164. [CrossRef] [PubMed]
9. Nolan, L.; Wit, A.; Dudziński, K.; Lees, A.; Lake, M.; Wychowański, M. Adjustments in gait symmetry with walking speed in trans-femoral and trans-tibial amputees. *Gait Posture* **2003**, *17*, 142–151. [CrossRef] [PubMed]
10. Goldfarb, M.; Lawson, B.E.; Shultz, A.H. Realizing the promise of robotic leg prostheses. *Sci. Transl. Med.* **2013**, *5*, 210ps15. [CrossRef]
11. Nolan, L.; Lees, A. The functional demands on the intact limb during walking for active trans-femoral and trans-tibial amputees. *Prosthet. Orthot. Int.* **2000**, *24*, 117–125. [CrossRef] [PubMed]
12. Ishmael, M.K.; Tran, M.; Lenzi, T. ExoProsthetics: Assisting above-knee amputees with a lightweight powered hip exoskeleton. In Proceedings of the 2019 IEEE 16th International Conference on Rehabilitation Robotics (ICORR), Toronto, ON, Canada, 24–28 June 2019; pp. 925–930. [CrossRef] [PubMed]

13. Keller, E.; Laubscher, C.; Gregg, R. Effects of a powered knee-ankle prosthesis on intact joint biomechanics across sustained activities of daily life. *IEEE DataPort* **2025**, *34*, 845–855. [CrossRef]
14. Martinez-Villalpando, E.C.; Mooney, L.; Elliott, G.; Herr, H. Antagonistic active knee prosthesis: A metabolic cost of walking comparison with a variable-damping prosthetic knee. In Proceedings of the Annual International Conference of the IEEE Engineering in Medicine and Biology Society, Boston, MA, USA, 30 August–3 September 2011; pp. 8519–8522. [CrossRef]
15. Tran, M.; Gabert, L.; Hood, S.; Lenzi, T. A lightweight robotic leg prosthesis replicating the biomechanics of the knee, ankle, and toe joint. *Sci. Robot.* **2022**, *7*, eabo3996. [CrossRef] [PubMed]
16. Browning, R.C.; Modica, J.R.; Kram, R.; Goswami, A. The effects of adding mass to the legs on the energetics and biomechanics of walking. *Med. Sci. Sports Exerc.* **2007**, *39*, 515–525. [CrossRef] [PubMed]
17. Panizzolo, F.A.; Galiana, I.; Asbeck, A.T.; Siviy, C.; Schmidt, K.; Holt, K.G.; Walsh, C.J. A biologically inspired multi-joint soft exosuit that can reduce the energy cost of loaded walking. *J. Neuroeng. Rehabil.* **2016**, *13*, 43. [CrossRef] [PubMed]
18. Ding, Y.; Panizzolo, F.A.; Siviy, C.; Malcolm, P.; Galiana, I.; Holt, K.G.; Walsh, C.J. Effect of timing of hip extension assistance during loaded walking with a soft exosuit. *J. Neuroeng. Rehabil.* **2016**, *13*, 87. [CrossRef] [PubMed]
19. Ding, Y.; Kim, M.; Kuindersma, S.; Walsh, C.J. Human-in-the-loop optimization of hip assistance with a soft exosuit during walking. *Sci. Robot.* **2018**, *3*, eaar5438. [CrossRef] [PubMed]
20. Lewis, C.L.; Ferris, D.P. Invariant hip moment pattern while walking with a robotic hip exoskeleton. *J. Biomech.* **2011**, *44*, 789–793. [CrossRef] [PubMed]
21. Seo, K.; Lee, J.; Lee, Y.; Ha, T.; Shim, Y. Fully autonomous hip exoskeleton saves metabolic cost of walking. In Proceedings of the 2016 IEEE International Conference on Robotics and Automation (ICRA), Stockholm, Sweden, 16–21 May 2016; pp. 4628–4635. [CrossRef]
22. Xiong, J.; Zhang, Y.; Leng, Y.; Xian, H.; Chen, C.; Wu, Y.; Zhuang, W.; Chen, X.; Fu, C. Future hip angle guided control: A concise and explicit assistance framework for hip exoskeleton. *IEEE/ASME Trans. Mechatron.* **2026**, *31*, 5100–5111. [CrossRef]
23. Cao, W.; Ma, Y.; Chen, C.; Zhang, J.; Wu, X. Hardware Circuits Design and Performance Evaluation of a Soft Lower Limb Exoskeleton. *IEEE Trans. Biomed. Circuits Syst.* **2022**, *16*, 384–394. [CrossRef] [PubMed]
24. Pruyn, K.; Murray, R.; Gabert, L.; Foreman, K.B.; Lenzi, T. Portable hip exoskeleton improves walking economy for stroke survivors. *Nat. Commun.* **2026**, *17*, 2771. [CrossRef] [PubMed]
25. Lee, H.-J.; Lee, S.-H.; Seo, K.; Lee, M.; Chang, W.H.; Choi, B.-O.; Ryu, G.-H.; Kim, Y.-H. Training for walking efficiency with a wearable hip-assist robot in patients with stroke: A pilot randomized controlled trial. *Stroke* **2019**, *50*, 3545–3552. [CrossRef] [PubMed]
26. Department of Veterans Affairs; Department of Defense. *VA/DoD Clinical Practice Guideline for Rehabilitation of Individuals with Lower Limb Amputation*; version 3.0; Department of Veterans Affairs and Department of Defense: Washington, DC, USA, 2024. Available online: https://healthquality.va.gov/HEALTHQUALITY/guidelines/Rehab/amp/LLA-CPG_2024-Guideline_final_20250110.pdf (accessed on 24 September 2026).
27. Kroes, C.M.; Schelhaas, R.; Dekker, R.; Geertzen, J.H.B.; Van Kammen, K.; Houdijk, H. Muscle morphology and function following a transfemoral amputation: A systematic review. *Can. Prosthet. Orthot. J.* **2026**, *9*, 47289. [CrossRef] [PubMed]
28. Poonsiri, J.; Dijkstra, P.U.; Geertzen, J.H.B. Fitting transtibial and transfemoral prostheses in persons with a severe flexion contracture: Problems and solutions—A systematic review. *Disabil. Rehabil.* **2022**, *44*, 3749–3759. [CrossRef] [PubMed]
29. Sanz-Morère, C.B.; Martini, E.; Meoni, B.; Arnetoli, G.; Giffone, A.; Doronzio, S.; Fanciullacci, C.; Parri, A.; Conti, R.; Giovacchini, F.; et al. Robot-mediated overground gait training for transfemoral amputees with a powered bilateral hip orthosis: A pilot study. *J. Neuroeng. Rehabil.* **2021**, *18*, 111. [CrossRef] [PubMed]
30. Sanz-Morère, C.B.; Martini, E.; Arnetoli, G.; Doronzio, S.; Giffone, A.; Meoni, B.; Parri, A.; Conti, R.; Giovacchini, F.; Friðriksson, Þ.; et al. Energy cost of transport in overground walking of a transfemoral amputee following one month of robot-mediated training. In *Wearable Robotics: Challenges and Trends*; Moreno, J.C., Masood, J., Schneider, U., Maufroy, C., Pons, J.L., Eds.; Springer: Cham, Switzerland, 2022; pp. 251–255. [CrossRef]
31. Koseki, K.; Yozu, A.; Takano, H.; Abe, A.; Yoshikawa, K.; Maezawa, T.; Kohno, Y.; Mutsuzaki, H. Gait training using the Honda Walking Assist Device for individuals with transfemoral amputation: A report of two cases. *J. Back. Musculoskelet. Rehabil.* **2020**, *33*, 339–344. [CrossRef] [PubMed]
32. Ishmael, M.K.; Archangeli, D.; Lenzi, T. Powered hip exoskeleton improves walking economy in individuals with above-knee amputation. *Nat. Med.* **2021**, *27*, 1783–1788. [CrossRef] [PubMed]
33. Ishmael, M.K.; Gunnell, A.; Pruyn, K.; Creveling, S.; Hunt, G.; Hood, S.; Archangeli, D.; Foreman, K.B.; Lenzi, T. Powered hip exoskeleton reduces residual hip effort without affecting kinematics and balance in individuals with above-knee amputations during walking. *IEEE Trans. Biomed. Eng.* **2023**, *70*, 1162–1171. [CrossRef] [PubMed]
34. Seroussi, R.E.; Gitter, A.; Czerniecki, J.M.; Weaver, K. Mechanical work adaptations of above-knee amputee ambulation. *Arch. Phys. Med. Rehabil.* **1996**, *77*, 1209–1214. [CrossRef] [PubMed]

35. Vito, M.; Aprigliano, F.; Arnetoli, G.; Doronzio, S.; Giffone, A.; Molino Lova, R.; Vitiello, N.; Micera, S. Counteracting Balance Loss in Transfemoral Amputees by Using an Active Pelvis Orthosis: A Case Series. In *8th European Medical and Biological Engineering Conference*; Jarm, T., Cvetkoska, A., Mahnič-Kalamiza, S., Miklavcic, D., Eds.; IFMBE Proceedings; Springer: Cham, Switzerland, 2021; Volume 80, pp. 294–305. [CrossRef]
36. Martini, E.; Sanz-Morère, C.B.; Livolsi, C.; Pergolini, A.; Arnetoli, G.; Doronzio, S.; Giffone, A.; Conti, R.; Giovacchini, F.; Friðriksson, Þ.; et al. Lower-limb amputees can reduce the energy cost of walking when assisted by an Active Pelvis Orthosis. In Proceedings of the 2020 8th IEEE RAS/EMBS International Conference for Biomedical Robotics and Biomechatronics (BioRob), New York, NY, USA, 29 November–1 December 2020; pp. 809–815. [CrossRef]
37. Livolsi, C.; Sanz-Morère, C.B.; Pergolini, A.; Giffone, A.; Giovacchini, F.; Friðriksson, Þ.; Alexandersson, A.; Macchi, C.; Trigili, E.; Crea, S.; et al. Enhancing walking performance with bilateral hip exoskeleton assistance in individuals with above-knee amputation. *IEEE Trans. Neural Syst. Rehabil. Eng.* **2024**, *32*, 2553–2563. [CrossRef] [PubMed]
38. Lee, J.; Seo, K.; Lim, B.; Jang, J.; Kim, K.; Choi, H. Effects of assistance timing on metabolic cost, assistance power, and gait parameters for a hip-type exoskeleton. In Proceedings of the IEEE International Conference on Rehabilitation Robotics (ICORR), London, UK, 17–20 July 2017; pp. 498–504. [CrossRef] [PubMed]
39. Pérez-Suárez, I.; Martín-Rincón, M.; González-Henríquez, J.J.; Fezzardi, C.; Pérez-Regalado, S.; Galván-Álvarez, V.; Juan-Habib, J.W.; Morales-Álamo, D.; Calbet, J.A.L. Accuracy and precision of the COSMED K5 portable analyser. *Front. Physiol.* **2018**, *9*, 1764. [CrossRef] [PubMed]
40. Camargo, J.; Ramanathan, A.; Flanagan, W.; Young, A. A comprehensive, open-source dataset of lower limb biomechanics in multiple conditions of stairs, ramps, and level-ground ambulation and transitions. *J. Biomech.* **2021**, *119*, 110320. [CrossRef] [PubMed]
41. Hussain, R.; Marmar, Z. Gait dataset of 14 Syrian above-knee amputees and 20 healthy subjects. *Data Brief.* **2021**, *38*, 107365. [CrossRef] [PubMed]
42. Panizzolo, F.A.; Freisinger, G.M.; Karavas, N.; Eckert-Erdheim, A.M.; Siviy, C.; Long, A.; Zifchock, R.A.; LaFiandra, M.E.; Walsh, C.J. Metabolic cost adaptations during training with a soft exosuit assisting the hip joint. *Sci. Rep.* **2019**, *9*, 9779. [CrossRef] [PubMed]

Disclaimer/Publisher's Note: The statements, opinions and data contained in all publications are solely those of the individual author(s) and contributor(s) and not of MDPI and/or the editor(s). MDPI and/or the editor(s) disclaim responsibility for any injury to people or property resulting from any ideas, methods, instructions or products referred to in the content.